Research Article

Reducing Electromagnetic Interference in Three-Level T-type Isolated Bidirectional DC-DC Converter Using a Snubber Circuit

Halime Hızarcı [a],* , Kemal Kalaycı [a] , Onur Demirel [b] , Uğur Arifoğlu [a]

[a]Department of Electrical and Electronic Engineering, Faculty of Engineering, Sakarya University, Sakarya 54187, Turkey
[b]Department of Electronic and Automation, Ahi Evran University, Kırşehir 40100, Turkey

ARTICLE INFO	ABSTRACT
	Electromagnetic interference is the main problem in high switching power converters like DC-DC converters. One of the solution methods for electromagnetic interference reduction is to design a snubber circuit. The snubber circuit is a practical method to reduce fluctuations caused by parasitic components from the layout and non-ideal characteristics of switching devices. An effective snubber circuit design increases the converter's efficiency and reduces EMI noise. In this paper, electromagnetic interference is reduced using different snubber circuits in a three-level T-type isolated bidirectional DC-DC converter. The converter is simulated in PSIM to see the effectiveness of the noise reduction with the snubber circuits. CISPR 25 standard is used for the compliance assessment in the study.

1. Introduction

Bidirectional DC-DC converters are used in the conversion of the different DC voltage levels, and they have great importance in fields such as electric vehicles, avionics, and renewable energy. High efficiency is demanded in power converter designs for higher power density and small size.

Since three-level topologies create lower voltage stress on switching devices than two-level topologies in bidirectional DC-DC converters, it has become widely used in bidirectional power transfer [1]. Three-level topologies are of two types; I-type Neutral-Point Clamped (NPC) and T-type NPC. The T-type NPC switch combination is more reliable than the I-type NPC switch combination. The two extra diodes found in the I-type NPC switch combination are not available in the T-type NPC switch combination. Therefore, the T-type NPC switch combination reduces conduction losses by shortening the current path. In the T-type NPC switch combination, the cost is lower as there are no two extra keys found in the I-type [2]–[5].

The high-frequency switching reduces converter size and increases efficiency; however, it also increases electromagnetic interference (EMI). Elimination of the noises is not completely possible, but the noise levels may be attenuated to certain levels [6].

The switching device in the DC-DC converter operating at high-frequency causes large *dv/dt* and *di/dt* fluctuations. The large fluctuations at the switching also cause high stress on the switches and power losses. The main source of the conducted and radiated emissions is the rapid changes of transient voltages and currents during turn-on and turn-off operations of the switches.

The main reason for V_{DS} ringing and spikes on a MOSFET is parasitic inductance in the DC-DC converters. High switching rates of the MOSFET cause high spikes in addition to long ringing durations. Unfortunately, high-frequency switching also generates EMI. Particularly, this problem is more noticeable in the designs with the high current levels. EMI noise currents propagate from the converter into the DC power source (i.e., battery). When the EMI noise exceeds certain levels in a circuit, the circuit will encounter malfunctions or errors. Moreover, the circuit will also affect the other circuits in the environment as a noise source.

Solving EMI problems at the design stage is more effective as it enables to curb post-processing solutions (internal or external filter design). Thus, noise problems will be solved without high test duration and costs [7].

A summary of the conducted EMI reduction techniques is given in Figure 1 [8]. There are two ways to reduce unintended noise in the power converters. The first one is the solution that makes an impedance path for the noise signal to reduce emissions from the main port. This solution can be provided with inside or external filtering. The second technique looks for a solution at the source of EMI noise. In this technique, EMI mitigation is possible at the beginning of the design process. So, EMI noise may be attenuate without extra filtering elements such as choke and filter capacitors.
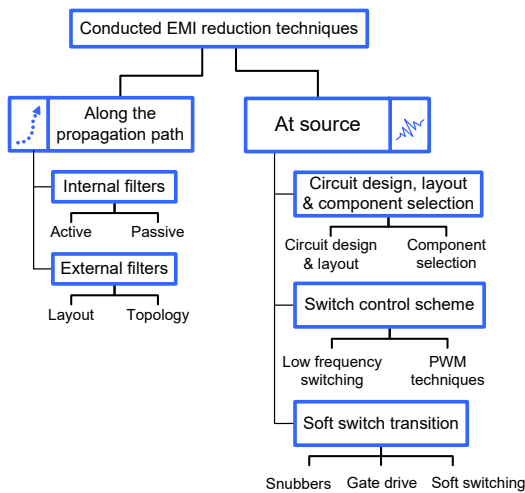

Figure 1. EMI reduction techniques [8]

There are several methods to solve EMI problems at the noise source. In a study conducted by Mihalic and Kos, pulse width modulation (PWM) and randomized PWM techniques are compared for noise reduction. According to the study, RPWM produces minimum EMI noise, and usage for the DC-DC converter is suitable [6]. A review study about conducted emission interference in non-isolated DC-DC power converters is presented in [9]. EMI reduction techniques such as soft switching, random modulation, and EMI filter design are summarized. It is seen that without the need for an EMI filter design, EMI noise may be reduced. However, sometimes the noise reduction is not adequate using the methods that solve problems at the source. In this case, an EMI filter design is required.

Yin et al. [10] have presented an EMI conduction modeling for buck converter using SPICE simulation and verified the model with measurement results in the domain. Any noise reduction method is not presented in the study. Subramanian and Govindarajan [11] propose a non-feedback

control technique using the concept of resonant parametric perturbation for EMI suppression. Iftikhar et al. [12] propose an LC input filter design to suppress EMI for boost converter and examine instability issues resulting from the filter and converter interaction.

One of the EMI noise reduction techniques is designing a snubber for the circuit as a sub-section of the soft-switching method. The RC snubber circuit reduces EMI in the converter without the need for an EMI filter design. As the volume and weight of the EMI filters are high in the converters, the converter without the EMI filter will have a high-power density [13].

The purpose of this paper is to show the effectiveness of the snubber in EMI reduction for the DC-DC converter. For this reason, a novel three-level T-type bidirectional DC-DC converter topology [14] is simulated without and with a snubber in PSIM. EMI noise spectra are obtained and compared with the CISPR 25 standard to see EMC compliance of the converter. It is seen that EMI noise may be reduced to some degree without the EMI filter's necessity.

2. Three-level T-type Bidirectional DC-DC Converter

Compared with the three-level I-type switch combination, the T-type switch combination has some advantages: high efficiency, symmetrical loss distribution, low harmonic pollution, less drive signal, etc. [15]. The T-type switch combination has already offered the best gain considering cost, reliability, input voltage, output power level, and efficiency. The analysis of the bidirectional three-level T-type DC-DC converter (Figure 2) in continuous current mode (CCM) operation was performed in [14].
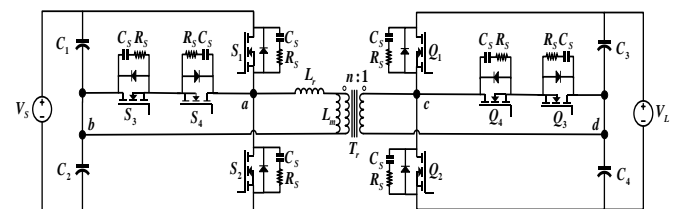

Figure 2. T-type bidirectional DC-DC converter topology using RC snubber circuit

However, EMI analysis of bidirectional T-type DC-DC converter has not been performed in the literature yet. In this study, the distortion in the switching voltage and current waveforms are measured, and the EMI noise measurement is made for four cases: without snubber, with RC snubber in horizontal switching elements, with the C- only snubber in all switching elements, and with RC snubber in all switching elements.
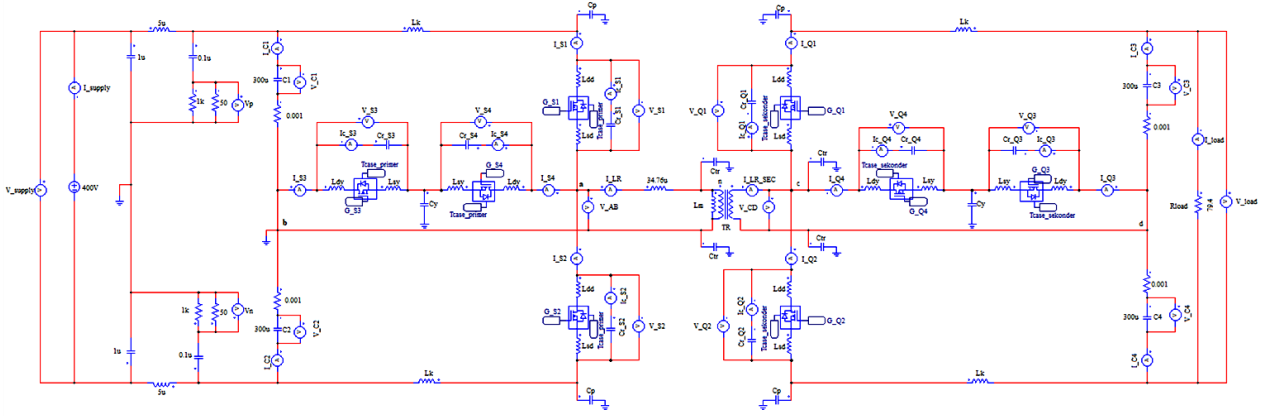
Figure 3. T-type DC-DC converter simulation in PSIM for all MOSFETs only have C snubber case

2.1. RC Snubber Circuit for the T-type DC-DC Converter

In the use of the snubber circuit, since the snubber capacitor will be discharged, dead-time must be left according to the commutating time. To prevent shoot-through over switches, 100 ns is left as the dead-time. We can determine the snubber capacitor value according to the operation steps in [16], [17]. The maximum snubber capacitor value is calculated as in (1)

$$C_{s\_max} = \frac{(I_{Lr}/3) \times t_{dead}}{\Delta V_{Cs}} = \frac{4.48 \times 100 \times 10^{-9}}{200} \tag{1}$$
$$= 2.24 nF$$

The snubber capacitor current (I_{cs}) at commutation times is one-third of the inductor current (I_{lr}). During the commutation times, the snubber capacitor voltage increased from 0V to 200V, from 200V to 400V, and decreased from 400V to 200V and from 200V to 0V. Snubber capacitor voltage variation (ΔV_{Cs}) is 200V.

The snubber capacitor value (Cs) was chosen as 2.2nF, which is the closest value to the maximum value.

According to the T-type circuit structure based on (2), dead-time selection can be found.

$$C_s \frac{\Delta V_{Cs}}{\Delta t} = I_{Cs} = \frac{I_{Lr}}{3} \tag{2}$$

For the snubber capacitor commuting time (t_{Cs}), CCM operation is evaluated by (3):

$$t_{Cs} = C_s \frac{\Delta V_{Cs}}{I_{Lr}/3} \tag{3}$$

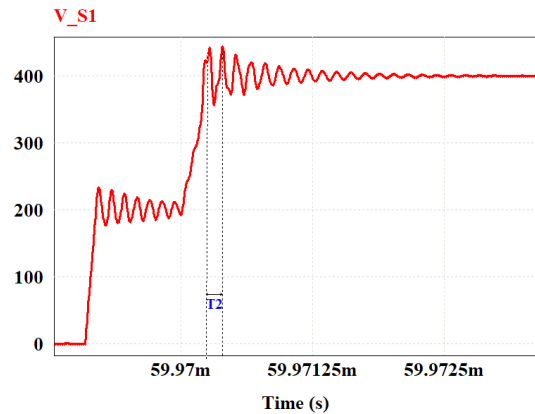If the snubber capacitor is selected 2.2 nF, the commuting time is obtained as in (4)

$$t_{Cs} = 2.2 \times 10^{-9} \frac{200}{4.48} = 98.21 \, ns \tag{4}$$

Since $t_{dead} > t_{cs}$ is required to ensure that the switching current and voltage do not overlap dangerously with each other.

The required calculation for determining the resistance value [18] of the RC snubber as follows.
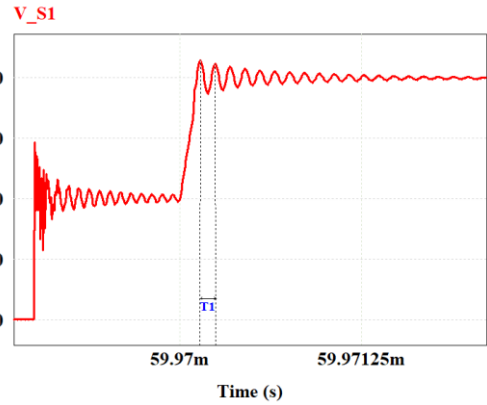
a)

b)

Figure 4. a) Switching voltage waveform (S$_1$) measurement without snubber circuit (case 1) b) Switching voltage waveform (S$_1$) measurement for all MOSFET only have C snubber (case 3)

As can be seen from Figure 4, the voltage ring period is T_1 in the snubberless state. In the case of switches that have the snubbers, the voltage ring period is T_2. Since the 2.2 nF is selected as the snubber capacitor, the approximate parasitic inductance value can be calculated with (5).

$$L_p = \frac{T_2^2 - T_1^2}{4\pi^2 C_{ext}} = \frac{(130.233n)^2 - (101.748n)^2}{4\pi^2 \times 2.2n} = 76.08 \, nH \tag{5}$$

Switch parasitic capacitance value (Cp) can be calculated by rearranging (5).

$$C_p = \frac{1}{4\pi^2 \times L_p \times f_1^2} = \frac{1}{4\pi^2 \times 76.08n \times (9.828M)^2} \quad (6)$$
$$= 3.447\,nF$$

When the damping ratio ζ is set to 1, the snubber resistance value can be calculated as in (7)

$$R_s = \frac{1}{2}\zeta\sqrt{\frac{L_p}{C_p}} = \frac{1}{2}\sqrt{\frac{76.08n}{3.447n}} = 2.349\,\Omega \quad (7)$$

The ESR of the 2.2nF capacitor value we have chosen is taken as 0.35 ohms in the simulation. As a result, 2 Ω is used as the snubber resistance in this study.

As the RC snubber circuit increases the power loss in the power converter, it is very important to set the optimal value of the snubber resistor. The efficiency of the converter should be considered designing a snubber. The schematic of the T-type DC-DC converter with the snubber circuits is given in Figure 3. The snubber circuits are added across the switches S_1, S_2, S_3, and S_4 on the primary and Q_1, Q_2, Q_3, and Q_4 on the secondary side.

Snubber is the sub-sections of soft switching transition and EMI reduction technique at the source. Proper design of the snubber circuit provides a reduction in EMI noise and minimizes the stress on the switches. Therefore, this technique is commonly used in power converter designs.

3. Conducted Emission Measurement

Electromagnetic compatibility (EMC) is the test that controls any product's compatibility with the other devices in the environment. The EMC test aims to operate the devices or systems without affecting and being affected by other devices or systems in the environment [19]. Conducted emission (CE) is electromagnetic disturbances produced by the device and propagate through power cords to the power grid or other systems. High levels of CE may cause unexpected operating conditions in the systems. So, the CE test is one of the EMC tests applied to products.

There are standards and directives to specify any device's compliance with its environment. The widely accepted standards are regulated by International Electrotechnical Commission (IEC), Comite International Special des Perturbations Radioelectrique (CISPR), Federal Communications Commission (FCC), and Verband Deutscher Elektrotechniker (VDE). These commissions recommend the permissible conducted and radiated EMI limits that products must comply with it. EMC measurement is realized in specific frequency bands, and this range is changing according to the standard.

3.1. CISPR 25 Standard

CISPR 25/EN 55025 [20] is an EMC standard for the equipment on vehicles and boats. The frequency range of the CISPR 25 standard is 0.15 MHz-108 MHz, and the allowable limits are given in Table 1.

Table 1. Limits for narrowband conducted disturbances on power input terminals (peak detector) [20]

Class	Levels in dBμV				
	0.15-0.3 MHz	0.53-2 MHz	5.9-6.2 MHz	30-54 MHz	70-108 MHz
1	90	66	57	52	42
2	80	58	51	46	36
3	70	50	45	40	30
4	60	42	39	34	24
5	50	34	33	28	18
Note: For 87 MHz to 108 MHz, add 6 dB to the level shown in the table.					

CISPR 25 Class 2 and Class 3 are used for the compatibility assessment in this study.

3.2. Line Impedance Stabilization Network (LISN)

The typical CE measurement setup is given in Figure 4 consists of LISN, EMI receiver, and ground plane.
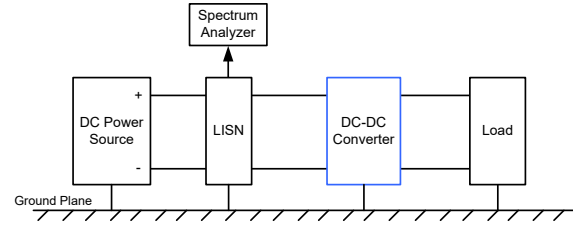

Figure 5. Typical measurement setup for conducted emission

In Figure 5, LISN is the circuit that provides a standardized impedance (50 Ω) between the source and equipment under test (EUT). Coupling between the measurement point of the EUT and the EMI receiver is provided with the LISN. The LISN eliminates the unwanted interference signals coming from the main power supply and prevents influencing the measurement.

In this study, LISN used for CISPR 25 automotive standard is given in Figure 6. In Figure 5, $L_1 = 5\,\mu H$, $C_1 = 0.1\,\mu F$, $C_2 = 0.1\,\mu F$, and $R_1 = 1\,k\Omega$.
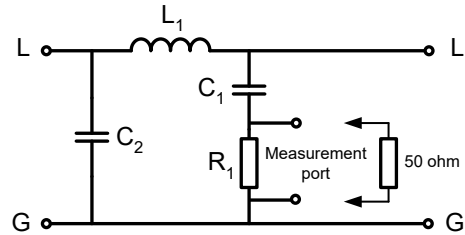

Figure 6. LISN scheme for CISPR 25 standard

EMI receiver is special test equipment in EMC test. It measures the electromagnetic signals through the signal detectors (peak (PK), quasi-peak (QP), and average (AVG)) given in the related standard. The ground plane is a conductive metal sheet essential to provide a reference plane for the CE's proper measurement.

4. Simulation Study

In this study, a 2 kW, 400 V/400 V three-level T-type

bidirectional DC-DC converter is used for EMI analysis. The converter is operated at full-load and in CCM operating mode. The simulation of the DC-DC converter is realized in PSIM software (given in Figure 3). The parasitic effects of the component are integrated into the circuit model for an accurate and realistic simulation. Circuit design and control parameters were determined using reference [11].

Important control parameters of the converter are selected as below.

- The switching frequency (f_s): 50 kHz
- The transformer conversion ratio is n=1. So, the voltage gain of the converter is 1.
- The duty cycles (D) of S_1, S_2, Q_1, Q_2 switches are 0.445, D of the other switches is 0.5.
- The phase shift between the driving signals of primary and secondary switches is 42.38°.
- A 100 ns dead-time is left before switches S_1, S_2, Q_1, Q_2 go into the turn on

The dead-time is chosen greater than the switching time of the MOSFET and the charging time of the snubber capacitor. The thermal model of IPW65R050CFD7A MOSFET is used as the switching device. The switching device is driven at 16/-4V. The gate turn-on resistance of the gate driver is 12 Ω, and the gate turn-off resistance is 6 Ω. While the initial junction temperature of MOSFET is 25°C, the primary and secondary case temperatures are entered in the model to increase to 36°C in operating conditions. The bulk capacitor values in primary and secondary sides are 300 µF, and the series resistance is 0.001 Ω. The inductance value is taken as $L_r = 34.76\ \mu H$ in order for the circuit to operate in CCM. The magnetization inductance of the transformer is $L_m = 500\ \mu H$. The output load is set at 79.4 Ω for the converter to work at 2 kW full load.

Parasitic inductor and capacitance values were determined according to the characteristics and inferences in [21]–[26]. Parasitic inductance with values $L_d = 5\ nH$, $L_s = 20\ nH$ is added to the drain and source legs of each MOSFET, respectively. Besides, parasitic inductance with a value of $L_k = 1.8\ nH$ is connected to the upper and lower arms of the primary and secondary circuits. Common mode capacitances are selected as $C_p = 5\ nF$ for the upper and lower arms in the primary and secondary circuits. $C_y = 5\ nF$ is chosen for horizontal MOSFETs. Also, $C_{tr} = 1\ nF$ parasitic capacities are added to the transformer ends.

In this study, four cases are considered for the EMC assessment of the DC-DC converter.

Case 1: Without snubber:

All MOSFETs have their output capacitance C_{oss} values of 0.05 nF.

Case 2: RC snubber only in horizontal MOSFETs

2.2 nF, 2 Ω snubber capacitors are connected to

horizontal MOSFETs. Vertical MOSFETs have their C_{oss} values of 0.05 nF.

Case 3: All MOSFETs only have C snubber

Snubber capacitors of 2.2 nF are connected to each MOSFET.

Case 4: Case with RC snubber in all MOSFETs

2.2 nF, 2 Ω snubber capacitors are connected.

Switching waveforms and EMI noise spectrum of the DC-DC converter for the cases are given in Figure 7, Figure 8, Figure 9, and Figure 10, respectively.
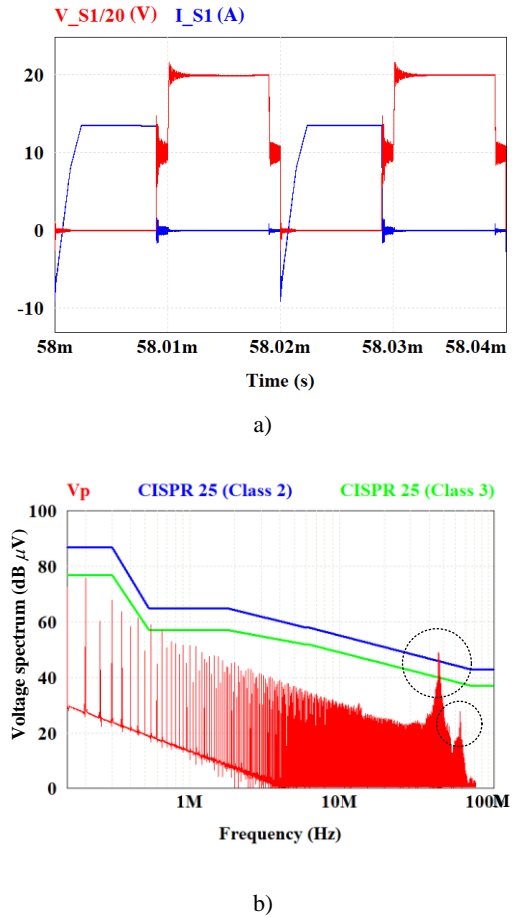

a)

b)

Figure 7. a) Switching waveforms (S_1) and b) EMI noise measurement without snubber circuit (case 1)

Figure 7 (a) shows the voltage and current waveforms of the S_1 switch in the snubberless case. While the S_1 switch is entering the turn-off state, it is required that the voltage increase from 0 V to 200 V. However, the voltage has increased to 295 V. So, distortion with a peak value of 95 V occurs. While the S_1 switch is required to increase from 200V to 400V, it has increased to 432.5 V. There is a distortion with a peak value of 32.5 V. Likewise, there is a 26 V fluctuation in the drop from 400 V to 200 V and a fluctuation of 35 V in the decrease from 200 V to 0 V.

For the EMI measurement, LISN is connected to phase and neutral lines, as seen in Figure 3. CISPR 25 Class 2 and Class 3 standard limits are used in the study. Figure 7 (b) shows the phase voltage (V_p) spectrum. According to EMI analysis, a 48.93 dBµV peak value at 46.15 MHz is

seen. Values of CISPR 25 Class 2 and Class 3 standard limits at the same frequency are 45.98 dBµV and 39.98 dBµV, respectively. As can be understood from the EMI noise measurements made without the snubber circuit, it does not meet the CISPR 25 Class 2 and Class 3 limits.
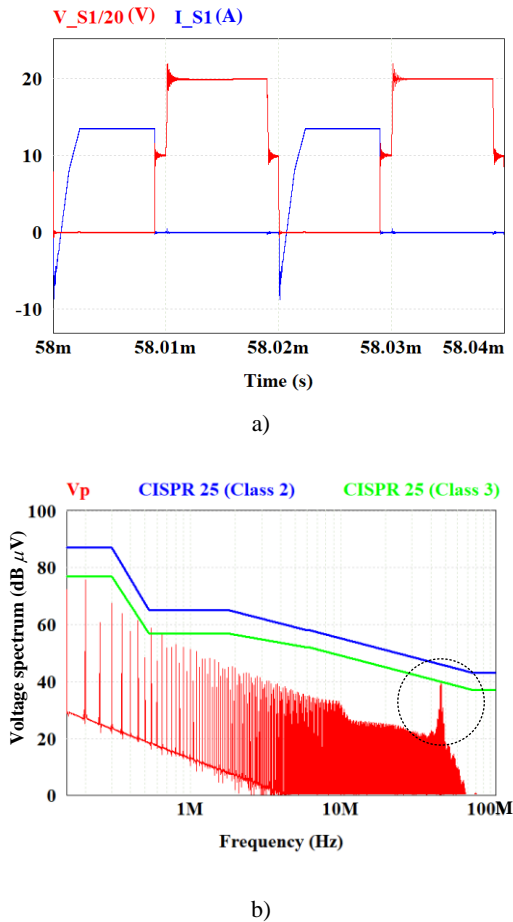
CISPR 25 Class 2 and Class 3 limits at the same frequency are 45.93 dBµV and 39.93 dBµV, respectively. As the V_p spectrum is lower than standard limits CISPR 25 Class 2 and Class 3 limits are both ensured in Case 2. Besides, the second peak that occurred at 64.35 MHz in Case 1 is reduced.
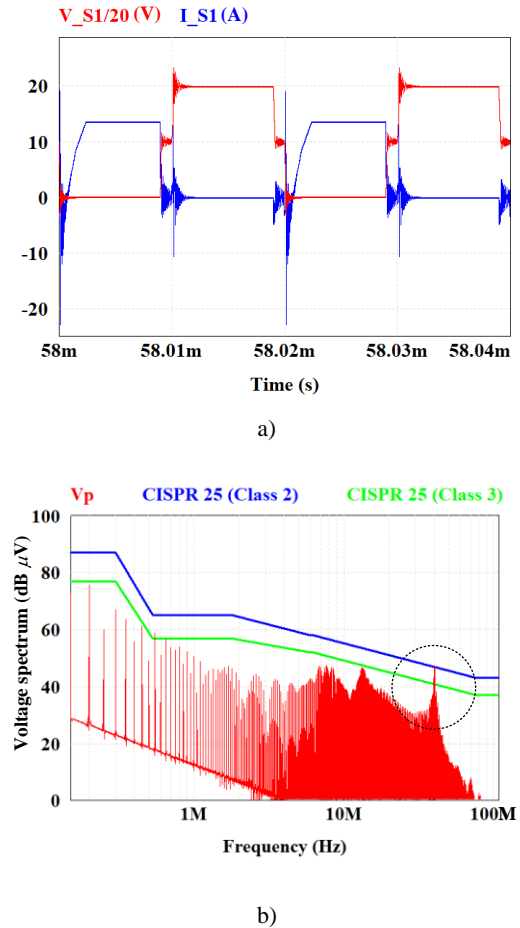

a)

b)

Figure 8. a) Switching waveforms (S₁) and b) EMI noise measurement with RC snubber circuit at only horizontal switches (case 2)

In Figure 8 (a), when the snubber is used only in horizontal switches (S₃, S₄, Q₃, Q₄), the voltage increased from 0 V to 231.2 V while the S₁ switch goes into the turn-off. However, it is required that the voltage increase from 0 V to 200 V. Therefore, the peak value of the distortion is measured as 31.2 V. While the S₁ switch is required to increase from 200 V to 400 V, it has increased to 439 V. Again, there is a distortion with a 39 V peak voltage. Likewise, there is a 20 V fluctuation in the decrease from 400 V to 200 V and a fluctuation of 7.5 V in the decrease from 200 V to 0 V. There is almost no distortion in the current waveform of the S₁ switch.

Compared to the snubberless case, only 6.5 V extra distortion occurs on the voltage waveform at the rise from 200 V to 400 V. All other voltages and current distortion values are better than the case of snubberless.

In Figure 8 (b), if snubber is used only in horizontal switches (S₃, S₄, Q₃, Q₄), the peak value of the V_p voltage spectrum at 46.6 MHz is 39.82 dBµV. Peak values of

a)

b)

Figure 9. a) Switching waveforms (S₁) and b) EMI noise measurement for the case C-only snubber at all switches (case 2)

Voltage and current waveform of S₁ switch for Case 3 (only 2.2 nF capacitor usage without snubber resistance in all switches) are given in Figure 9 (a). Furthermore, Figure 9 (b) shows EMI measurement results. Although using a capacitor-only snubber is generally not recommended in EMC designs, it is considered in the study to see effects on the switching transitions. Capacitor-only snubber is not a suggested design approach because a series resistor is required to limit the discharge current of the snubber capacitor [27]. The series resistor with the capacitor also protects the switch.

In Figure 9 (b), when capacitor-only snubber is used in all switching devices, EMI noise analysis is performed. The peak value of the V_p at 40.3 MHz is measured as 47.29 dBµV. In this case, the CISPR 25 Class 2 standard is not be achieved with a difference of 0.5 dBµV. On the other hand, CISPR 25 Class 3 standard is also not be met. According to the measurements made without snubber, an

improvement of roughly 1.64 dBµV is achieved in the peak value of EMI noise.

In Figure 10 (a) and (b), voltage and current waveform of S_1 switch and frequency spectrum of V_p for Case 4 (if a 2.2 nF, 2 Ω RC snubber is used in all switches) are given, respectively.
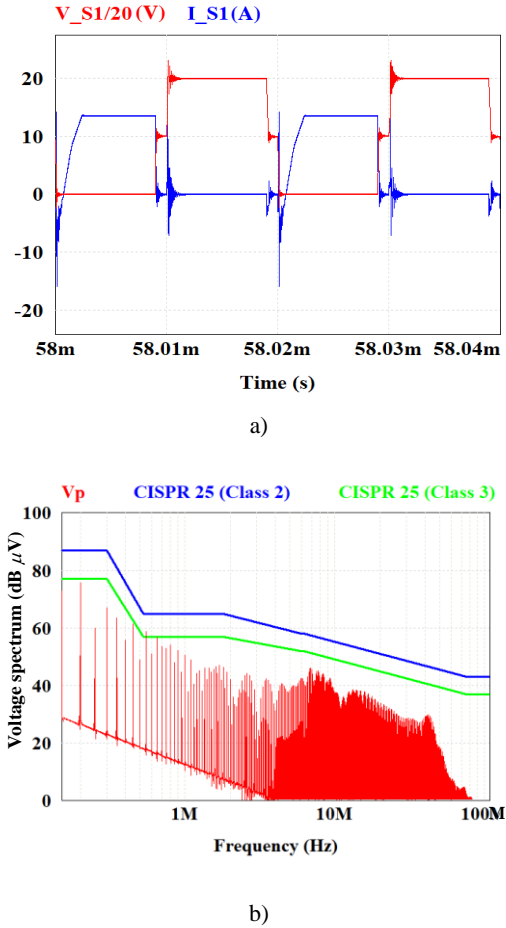

a)

b)

Figure 10. a) Switching waveforms (S_1) and b) EMI noise measurement with RC snubber circuit at all switches (case 4)

Figure 10 (b) shows that CISPR 25 Class 2 and Class 3 standards are met using RC snubber in all switching devices. It can be said that using RC snubber in all switches shows the best performance among all cases in terms of EMI.

As a result of this study, Figure 7 (a) and Figure 10 (a) show the switching waveform for snubberless and RC snubber cases across all switches. The difference between the damping of the ringing voltage across S_1 is obvious. As a result, in addition to reducing EMI noise, the snubber reduces the high ringing voltage and provides low switching losses for higher efficiency.

A summary table is presented in Table 2 to show voltage distortion.

Table 2. Voltage distortion according to the S_1 switch transition

	Voltage distortion			
S_1 switch transition	Case 1	Case 2	Case 3	Case 4
0 V→200 V	95 V	31.2 V	33.2 V	27.7 V
200 V→400 V	32.5 V	39 V	67 V	60.9 V
400 V→200 V	26 V	20 V	21 V	19 V

| 200 V→0 V | 35 V | 7.5 V | 55 V | 31 V |

Compared to Case 1 (without snubber) with Case 2 (only horizontal snubber) in Table 3, the distortion is 6.5 V higher when the voltage wave increases from 200V to 400 V. All other voltages and current distortion values are better than the case of snubberless. In the case of RC snubber only in horizontal switches, distortion is reduced in transition times. When RC snubber is used in all switches, it shows the best performance in the transition times (from 0 V to 200 V and from 400 V to 200 V). However, it should be kept in mind that the efficiency is lower than the RC snubber only in horizontal switches due to the use of RC snubber in all switches.

Adding a snubber circuit will also affect the efficiency of the converter. An assessment of all cases is given in Table 3.

Table 3. Comparison of the cases in terms of power loss and converter efficiency

	Switching losses (W)	Conduction losses (W)	Total losses (W)	Efficiency (%)
Snubberless	3.1725	19.43	47.9425	97.6
Horizontal RC Snubber	0.595	19.265	44.385	97.78
Capacitor-only snubber	2.06	20.24	47.52	97.62
RC Snubber	1.59	20.13	46.77	97.66

Switching, conduction, total losses, and efficiency for four cases resulting from the PSIM thermal analysis simulation are given in Table 3. This table gives the measurement of switching and conduction losses depending on current and voltage of the switching devices. Total losses also include inductor and transformer losses.

In terms of switching losses, conduction losses, and efficiency, the best performance has been achieved only when RC snubber is used in horizontal MOSFETs. The use of snubber appears to reduce switching losses. It is seen that conduction losses increase when only C and RC snubbers are used in vertical switches. However, switching losses are reduced in cases where an RC snubber circuit is used.

Table 4. Comparison of the cases in terms of switch RMS currents

Cases / Switches	Case 1 (RMS Current)	Case 2 (RMS Current)	Case 3 (RMS Current)	Case 4 (RMS Current)
S1	8.244A	8.238A	8.485A	8.308A
S2	8.316A	8.392A	9.827A	8.834A
S3	3.912A	3.483A	4.099A	3.44A
S4	3.853A	4.079A	5.809A	4.41A
Q1	8.47A	8.404A	8.548A	8.44A
Q2	8.5A	8.435A	8.901A	8.582A
Q3	4.154A	3.906A	4.139A	3.769A
Q4	4.162A	3.992A	4.445A	3.947A

The conduction loss for the DAB converter popular in bidirectional converters is reviewed in [28], [29], it is seen that the conduction losses vary in direct proportion to the

square of the switch RMS current. When calculating the conduction losses, the drain-source on resistance $R_{ds}(on)$ of the MOSFET is the same for all cases. However, switches RMS current is different for all cases. The RMS currents in vertical switches (S_1, S_2, Q_1, Q_2) are almost twice that of horizontal switches (S_3, S_4, Q_3, Q_4) at Table 4. Especially in vertical switches (S_1, S_2, Q_1, Q_2), it is seen that the RMS currents are higher in Cases 3 and 4 than in Cases 1 and 2. Since the switch RMS currents in Cases 3 and 4 will be squared when calculating the conduction loss, it confirms that the conduction losses of Cases 3 and 4 in Table 4 are higher than Cases 1 and 2.

As a result, EMI attenuation is provided with a snubber circuit in the high-frequency region in this study. Snubber circuit reduces EMI by damping voltage and current ringings. Thus, it presents an opportunity to mitigate the EMI noise without the need for extra filtering elements to some degree. This situation is invaluable for the converter design, especially in electric vehicles with limited space and volume.

5. Conclusions

This paper proposes an EMI reduction technique for the T-type bidirectional DC-DC converter using a snubber circuit. It is also seen that the snubber circuit reduces the ringing voltage of switches and increases the efficiency of the converter. The study aims to attenuate the EMI noise without using an EMI filter with bulky elements like a choke. The converter's simulation model is built-in PSIM, and CISPR 25 automotive standard is used for the EMC measurement.

In the case of RC snubber in all switches, the efficiency is low even if EMI standards are met. The best performance in providing efficiency and EMI standards has been achieved only when RC snubber is used in horizontal switches.

Acknowledgment

References

[1] P. Liu, C. Chen, S. Duan, and W. Zhu, "Dual Phase-Shifted Modulation Strategy for the Three-Level Dual Active Bridge DC–DC Converter," *IEEE Transactions on Industrial Electronics*, vol. 64, no. 10, pp. 7819–7830, Oct. 2017, doi: 10.1109/TIE.2017.2696488.

[2] K. Kalayci, O. Demirel, and U. Arifoğlu, "İki Yönlü Üç Seviyeli T-Tipi DA-DA Dönüştürücünün Süreksiz Akım Modundaki Analizi," 2019.

[3] W. Wu, F. Wang, and Y. Wang, "A novel efficient T type three level neutral-point-clamped inverter for renewable energy system," *2014 International Power Electronics Conference, IPEC-Hiroshima- ECCE Asia 2014*, pp. 470–474, 2014, doi: 10.1109/IPEC.2014.6869625.

[4] T. P. V. G. Inverter, "Study of Passivity-Based Decoupling Control of," vol. 64, no. 9, pp. 7542–7551, 2017.

[5] P. Zhou and Q. Chen, "Power Losses in T-type and NPC Inverters with SHEPWM Strategy," vol. 4, pp. 562–566, 2017.

[6] F. Mihalič and D. Kos, "Reduced conductive EMI in switched-mode dc-dc power converters without EMI filters: PWM versus randomized PWM," *IEEE Transactions on Power Electronics*, vol. 21, no. 6, pp. 1783–1794, 2006, doi: 10.1109/TPEL.2006.882910.

[7] F. A. Kharanaq, A. Emadi, and B. Bilgin, "Modeling of Conducted Emissions for EMI Analysis of Power Converters: State-of-the-Art Review," *IEEE Access*, vol. 8, pp. 189313–189325, 2020, doi: 10.1109/ACCESS.2020.3031693.

[8] K. Mainali and R. Oruganti, "Conducted EMI Mitigation Techniques for Switch-Mode Power Converters: A Survey," *IEEE Transactions on Power Electronics*, vol. 25, no. 9, pp. 2344–2356, Sep. 2010, doi: 10.1109/TPEL.2010.2047734.

[9] S. Natarajan, T. Sudhakar Babu, K. Balasubramanian, U. Subramaniam, and D. J. Almakhles, "A State-of-the-Art Review on Conducted Electromagnetic Interference in Non-Isolated DC to DC Converters," *IEEE Access*, vol. 8, pp. 2564–2577, 2020, doi: 10.1109/ACCESS.2019.2961954.

[10] W. Yin, Z. Ming, T. Wen, and C. Wu, "Switching converter EMI conduction modelling and verification," *Electronics Letters*, vol. 55, no. 10, pp. 587–589, May 2019, doi: 10.1049/el.2019.0050.

[11] A. Subramanian and U. Govindarajan, "Analysis and mitigation of conducted EMI in current mode controlled DC–DC converters," *IET Power Electronics*, vol. 12, no. 4, pp. 667–675, Apr. 2019, doi: 10.1049/iet-pel.2018.5322.

[12] M. U. Iftikhar, D. Sadarnac, and C. Karimi, "Conducted EMI Suppression and Stability Issues in Switch-mode DC-DC Converters," in *2006 IEEE International Multitopic Conference*, Dec. 2006, pp. 389–394. doi: 10.1109/INMIC.2006.358198.

[13] H. Ertl, T. L. P. W. M. Rectifier, M. Hartmann, S. Member, H. Ertl, and J. W. Kolar, "EMI Filter Design for a 1 MHz, 10 kW," vol. 26, no. 4, pp. 1192–1204, 2011.

[14] O. Demirel, U. Arifoglu, and K. Kalayci, "Novel three-level T-type isolated bidirectional DC–DC converter," *IET Power Electronics*, vol. 12, no. 1, pp. 61–71, Jan. 2019, doi: 10.1049/iet-pel.2018.5680.

[15] J. Wang, X. Mu, and Q.-K. Li, "Study of Passivity-Based Decoupling Control of T-NPC PV Grid-Connected Inverter," *IEEE Transactions on Industrial Electronics*, vol. 64, no. 9, pp. 7542–7551, Sep. 2017, doi: 10.1109/TIE.2017.2677341.

[16] D. G. Bandeira and I. Barbi, "A T-Type Isolated Zero Voltage Switching DC-DC Converter with Capacitive Output," *IEEE Transactions on Power Electronics*, vol. 32, no. 6, pp. 4210–4218, 2017, doi: 10.1109/TPEL.2016.2600654.

[17] D. G. Bandeira, T. B. Lazzarin, and I. Barbi, "High Voltage Power Supply Using a T-Type Parallel Resonant DC-DC Converter," *IEEE Transactions on Industry Applications*, vol. 54, no. 3, pp. 2459–2470, 2018, doi: 10.1109/TIA.2018.2792446.

[18] F. S. Corporation, "AN-4162 — Switch Node Ring Control in Synchronous Buck Regulators," 2013.

[19] Henry W. Ott, *Electromagnetic Compatibility Engineering*. John Wiley & Sons, 2009.

[20] International Electrotechnical Commission (IEC), "CISPR 25:2016- Vehicles, boats and internal combustion engines – Radio disturbance characteristics – Limits and methods of measurement for the protection of on-board receivers," 2016.

[21] Y. Liu, Z. Zhao, W. Wang, and J. S. Lai, "Characterization and Extraction of Power Loop Stray Inductance with SiC Half-Bridge Power Module," *IEEE Transactions on Electron Devices*, vol. 67, no. 10, pp. 4040–4045, 2020, doi: 10.1109/TED.2019.2962571.

[22] B. T. Deboi, A. N. Lemmon, B. W. Nelson, C. D. New, and D. M. Hudson, "Improved Methodology for Parasitic Characterization of High-Performance Power Modules," *IEEE Transactions on Power Electronics*, vol. 35, no. 12, pp. 13400–13408, 2020, doi: 10.1109/TPEL.2020.2992332.

[23] S. Hu, M. Wang, Z. Liang, and X. He, "A Frequency-Based Stray Parameter Extraction Method Based on Oscillation in SiC MOSFET Dynamics," *IEEE Transactions on Power Electronics*, vol. 36, no. 6, pp. 6153–6157, 2021, doi: 10.1109/TPEL.2020.3033801.

[24] C. Wang, J. Zheng, G. Wang, W. Gao, and Q. Hua, "Parasitic effects analysis of bonding wires bonding parameter of intelligent power modules for three-phase motor control

applications," *Journal of Physics: Conference Series*, vol. 1607, no. 1, 2020, doi: 10.1088/1742-6596/1607/1/012036.

[25]   K. Wada, "Circuit implementation of power converter for high-speed switching operations," *Chinese Journal of Electrical Engineering*, vol. 4, no. 3, pp. 47–52, 2019, doi: 10.23919/cjee.2018.8471289.

[26]   L. Popova *et al.*, "Stray inductance estimation with detailed model of the IGBT module," *2013 15th European Conference on Power Electronics and Applications, EPE 2013*, 2013, doi: 10.1109/EPE.2013.6631852.

[27]   Henry W. Ott, *Electromagnetic Compatibility Engineering*. John Wiley & Sons, 2009.

[28]   F. Krismer and J. W. Kolar, "Closed form solution for minimum conduction loss modulation of DAB converters," *IEEE Transactions on Power Electronics*, vol. 27, no. 1, pp. 174–188, 2012, doi: 10.1109/TPEL.2011.2157976.

[29]   W. Han, R. Ma, Q. Liu, and L. Corradini, "A conduction losses optimization strategy for DAB converters in wide voltage range," *IECON Proceedings (Industrial Electronics Conference)*, pp. 2445–2451, 2016, doi: 10.1109/IECON.2016.7793784.